University Library

MINERVA ACCESS

A gateway to Melbourne's research publications

Minerva Access is the Institutional Repository of The University of Melbourne

Author/s:
Parker, LJ;Bocedi, A;Ascher, DB;Aitken, JB;Harris, HH;Lo Bello, M;Ricci, G;Morton, CJ;Parker, MW

Title:
Glutathione transferase P1-1 as an arsenic drug-sequestering enzyme

Date:
2017-02-01

Citation:
Parker, L. J., Bocedi, A., Ascher, D. B., Aitken, J. B., Harris, H. H., Lo Bello, M., Ricci, G., Morton, C. J. & Parker, M. W. (2017). Glutathione transferase P1-1 as an arsenic drug-sequestering enzyme. Protein Science, 26 (2), pp.317-326. https://doi.org/10.1002/pro.3084.

Persistent Link:
https://hdl.handle.net/11343/292224

Glutathione transferase P1-1 as an arsenic drug-sequestering enzyme

Lorien J Parker,[1,2] Alessio Bocedi,[3] David B Ascher,[1] Jade B Aitken,[4] Hugh H Harris,[5] Mario Lo Bello,[6] Giorgio Ricci,[3] Craig J Morton,[1,7] and Michael W Parker[1,2,7*]

[1]ACRF Rational Drug Discovery Centre, St. Vincent's Institute of Medical Research, Fitzroy, Victoria 3065, Australia

[2]Department of Biochemistry and Molecular Biology, Bio21 Molecular Science and Biotechnology Institute, The University of Melbourne, Parkville, Victoria 3010, Australia

[3]Department of Chemical Sciences and Technologies, University of Rome "Tor Vergata", Rome 00133, Italy

[4]School of Chemistry, The University of Sydney, New South Wales 2006, Australia

[5]Department of Chemistry, The University of Adelaide, South Australia 5005, Australia

[6]Department of Biology, University of Rome “Tor Vergata”, Rome 00133, Italy

[7]Co-senior authors

*Correspondence to: Michael Parker, St. Vincent's Institute of Medical Research, Fitzroy, Victoria 3065, Australia. Tel. +61 3 9231 2499. Fax +61 3 9416 2676. E-mail: mparker@svi.edu.au

Running title: Glutathione transferase arsenic complexes

Manuscript pages: 26 (incl. one Table); Figures: 4; Supp pages: 12 (incl. two tables)

Supplementary file: SI-final.pdf

This is the author manuscript accepted for publication and has undergone full peer review but has not been through the copyediting, typesetting, pagination and proofreading process, which may lead to differences between this version and the Version record. Please cite this article as doi:10.1002/pro.3084.

This article is protected by copyright. All rights reserved.

Abstract: Arsenic-based compounds are paradoxically both poisons and drugs. Glutathione transferase (GSTP1-1) is a major factor in resistance to such drugs. Here we describe using crystallography, X-ray absorption spectroscopy, mutagenesis, mass spectrometry and kinetic studies how GSTP1-1 recognizes the drug phenylarsine oxide (PAO). In conditions of cellular stress where glutathione (GSH) levels are low, PAO crosslinks C47 to C101 of the opposing monomer, a distance of 19.9 Å, and causes a dramatic widening of the dimer interface by ~10 Å. The GSH conjugate of PAO, which forms rapidly in cancerous cells, is a potent inhibitor (K_i=90 nM) and binds as a di-GSH complex in the active site forming part of a continuous network of interactions from one active site to the other. In summary, GSTP1-1 can detoxify arsenic-based drugs by sequestration at the active site and at the dimer interface, in situations where there is a plentiful supply of GSH, and at the reactive cysteines in conditions of low GSH.

Keywords: arsenic; glutathione transferases; inhibitors; resistance; X-ray crystallography

Impact statement: Here we show how an arsenic-based drug is recognized by the detoxifying enzyme GSTP1-1. We show that GSTP1-1 can detoxify arsenic-based drugs by sequestration and that the glutathione conjugate of phenylarsine oxide is one of the most potent inhibitors of GSTP1-1 known. This work provides a detailed mechanism for GST-based cellular resistance to such drugs and suggests new ways to inhibit GSTP1-1, an enzyme overexpressed in certain cancers.

Accepted Article

This article is protected by copyright. All rights reserved.

Accepted Article

Introduction

Glutathione transferases (GSTs; EC 2.5.1.18) are a key part of the antioxidant response system.[1,2] Their principal mode of detoxification is through catalyzing the conjugation of target compounds to glutathione (GSH) as a first step in the removal of toxins from cells. In addition, GSTs can also protect cells by binding toxic compounds, through non-catalytic sequestration mechanisms. Due to the high expression levels of GSTs in many cells, this particular ligandin function may contribute to toxin resistance more significantly than previously considered. GSTs have been strongly implicated in various cancers; for example, in several tumor cell lines there is substantial overexpression of these enzymes following exposure to anti-tumor drugs.[1-3] Acquired resistance, which eventually arises in patients after an initial period of successful anti-cancer treatment, has been related in some cases to the presence of GST enzymes.[4]

Arsenic is a human carcinogen causing cancers of the skin, lung, bladder, liver and kidney after long-term exposure. Toxic exposure to arsenic is a serious health problem in some parts of the world where it occurs either naturally or as a pollutant.[5] Although arsenic is well known for its properties as a human carcinogen, arsenicals have also been used as therapeutic agents for thousands of years.[6,7] Up until the early 1900s arsenic was used as the primary anti-leukemic agent until it was replaced by radiation therapy and more modern chemotherapy. Arsenicals made a comeback in the early 1970s when they were used successfully for the treatment of acute promyelocytic leukemia (APL). Arsenic trioxide (As_2O_3, Trisenox™) was approved for treatment of APL in 2000 for patients who fail to respond to other chemotherapy methods or have relapsed disease.[8] This recent success has prompted researchers to consider arsenic's application in the treatment of other malignant disorders including chronic lymphocytic leukemia, multiple myeloma[9,10] and solid tumors such as neuroblastoma,[11] gastric,[12] and cervical tumors.[13]

Cells can develop tolerance to arsenicals[14-16] and a correlation between GSTP1-1 overexpression and development of resistance to arsenicals has been described by a

This article is protected by copyright. All rights reserved.

number of workers. For example, the level of arsenic resistance in an arsenic-resistant mammalian cell line is correlated with expression levels of GSTP1-1 and GST inhibitors markedly decrease cell resistance to the metalloid.[17] It has been shown that the enzyme is directly involved in excretion of arsenic from cells.[18] Furthermore, acquired self-tolerance to arsenic in chronically exposed cells is associated with increased expression of GSTP1-1 and multi-drug resistance transporters.[19] Inhibition of the enzyme markedly increases arsenic accumulation and arsenic toxicity, indicating the enzyme's upregulation is critical for acquired tolerance in cells chronically exposed to arsenic.[19] GSTP1-1 has been shown to block As_2O_3-induced apoptosis in leukemia, prostate cancer and lymphoma cells.[20-22] *In vivo* studies have shown that GSH serves as a reducing agent for the conversion of arsenate to arsenite and that GST activity is involved in the metabolism of arsenic by catalyzing the formation of arsenic-GSH conjugates.[23,24] The tri-GSH conjugate $As(GS)_3$, is recognized and pumped out of the cell by multi-drug resistant pump 1. Leslie and co-workers showed that GSTP1-1 was required for transport of As(III) (plus GSH) providing substantive evidence that the formation of $As(GS)_3$ might be catalyzed by GSTP1-1.[25]

The organic arsenical, phenylarsine oxide (PAO), is a membrane-permeable phosphotyrosine phosphatase inhibitor that is active in hematopoietic cells.[26] Several groups have reported the cytotoxic effects of PAO in hematological malignancies.[26-28] The cytotoxic effect of PAO is nine times higher than As_2O_3 and this toxicity does not weaken towards As_2O_3-resistant cell lines.[29] These results suggested that PAO may be a promising new agent for the treatment of APL, particularly for APL patients who are resistant and refractory to As_2O_3 treatment. However, PAO's high toxicity and non-selectivity for cancer cells over normal cells are drawbacks to be overcome in any drug development program. Recently, an analogue of PAO (4-(*N*-(*S*-glutathionylacetyl)amino)phenylarsonous acid) has been tested in Phase I clinical trials for solid tumors that are refractory to standard therapy.[30]

This article is protected by copyright. All rights reserved.

Accepted Article

It is now well established that in human cancers, arsenic detoxification is performed by the GST/GSH detoxification system. However, the interaction of GSTP1-1 with arsenic-based drugs is surprisingly poorly characterized. Here we describe crystallographic, X-ray absorption spectroscopy, mass spectrometry, mutagenesis and kinetic studies of GSTP1-1's interactions with PAO. A crystal structure of PAO bound to GSTP1-1 in the absence of GSH, shows the region corresponding to helix α2, which contains the C47 residue, is disordered, consistent with PAO interacting with this reactive cysteine and causing the displacement of this region from its usual helical conformation. Binding is associated with a dramatic opening of the V-shaped dimer cleft. Furthermore, the extended X-ray absorption fine structure (EXAFS) and crystallographic studies suggest that PAO can crosslink C47 of one monomer to C101 of the neighboring monomer. Kinetic studies reveal that the GSH adduct of PAO binds in the active site of the enzyme and is one of the most potent inhibitors of GSTP1-1 so far described in the literature. The crystal structure of the PAO complex, in the presence of GSH, reveals that PAO binds as a di-GSH-phenyl arsenic complex at the active site of the enzyme. In addition, PAO interacts at the dimer interface with C101 of either subunit resulting in the formation of a continuous network of interactions that spans from the active site to the other. This is the first report of a GSTP1-1 inhibitor that can simultaneously block known ligand binding sites in both the active sites and dimer interface. Overall, the structures reveal that GSTP1-1, in the presence of GSH, can detoxify PAO in two ways: by binding di-GSH-phenyl arsenic at the G-site and by sequestering PAO alone at the dimer interface. In the absence of GSH, detoxification occurs through binding to the two reactive cysteine residues, C47 and C101. The structures provide a basis for the development of GST inhibitors that block all these sequestration modalities.

Results

The di-GSH adduct of PAO is a potent inhibitor of GSTP1-1

This article is protected by copyright. All rights reserved.

In healthy and cancerous cells GSH is present at millimolar concentrations. Thus we first explored how human GSTP1-1 recognizes PAO in the presence of its substrate GSH. In the presence of 1 mM GSH and sub-stoichiometric amounts of PAO (0.1 mM) at pH 6.5, the $PA(GS)_2$ complex is rapidly formed in a few seconds ($t_{1/2} < 1$ s). The complex is characterized by a typical UV spectrum with a maximum at 210 nm and a shoulder at 273 nm (ε_M = 2,500 $M^{-1}cm^{-1}$) [Fig. 1(A)]. The instability constant of the complex (K_{inst}), calculated as described in Materials and Methods section, is 1.6 x 10^{-9} M^2. When incubated with GSTP1-1, this compound behaves as a strong competitive inhibitor of GSTP1-1 toward GSH (K_i = 90 nM) (Table 1).

To verify the possible involvement of the two highly reactive cysteines (C47 and C101)[31] in the binding of the $PA(GS)_2$ complex, we measured the K_i values of the corresponding serine mutants of these two residues. The study suggests no direct interaction occurs between the mutated residues and the complex (Table 1). In fact, the decreased affinity of the complex in these mutants is quantitatively similar to the loss of affinity for GSH in both mutants.

Mass spectrometry reveals two adducts in the GSTP1-1 PAO GSH complex

In the presence of GSH two reaction species with GSTP1-1 were observed by mass spectrometry: a minor species with mass of 458.58 Da and a major species of 765.33 Da (Fig. S1). The former corresponds to a monoglutathionylated species of PAO whereas the latter corresponds to the diglutathionylated species of PAO.

Crystal structure of the GSTP1-1 PAO GSH complex reveals multiple binding sites

We determined the crystal structure of the enzyme in complex with PAO and GSH to a resolution of 1.5 Å. The structure reveals that PAO interacts with GSTP1-1 at two different sites [Fig. 2(A,B)]. In the active site, PAO is observed as the di-GSH phenyl arsenic complex [Fig. 2(C)]. One of the GSH ligands, GSH1, binds in the G-site in the same way,

This article is protected by copyright. All rights reserved.

Accepted Article

with the same interactions, as seen in other GST-GSH complexes.[32,33] The second GSH ligand, GSH2, binds in the active site in a head-to-tail direction with respect to the first GSH ligand. The GSH in the GSH2 site has a higher average temperature factor for its terminal glutamyl moiety (39 Å^2) compared with the G-site GSH (21 Å^2) which reflects the increased flexibility of this moiety and the relatively few contacts it makes with the protein as indicated by incomplete electron density [Fig. 2(C)]. The glycyl carboxylate moiety forms a salt bridge with the side-chain of Arg13 and there are numerous van der Waals interactions with Ile104 and Tyr108. The phenyl group of the arsenic complex stacks between the aromatic rings of Phe8 and Tyr108 (distance between centroids of 4.5 Å and 6 Å, respectively) as well as forming van der Waals interactions with the main-chain of Gly205 and the side-chain of Val10 [Fig. 2(C)]. The arsenic atom is covalently bound through the sulfur atoms of the two GSH molecules, as well as the phenyl ring, and is within vicinity of the hydroxyl of Tyr108 (3.2 Å). GSH2 makes a water-mediated interaction with Asp98 from the other subunit. GSH1 makes water-mediated interactions with residues such as Pro53, Gln64, Asn66 and Glu97 in addition to the usual protein interactions seen in other GSH bound GST structures, (Fig. S2).

Two arsenic binding sites were also identified at the dimer interface, covalently bound to C101 of each subunit [Fig. 2(A,B)]. Reaction of PAO with a single thiol group would lead to a phenylhydroxy-arsene complex. There was some additional electron density attached to the arsenic peaks that was modeled as the phenyl moieties. The location of the hydroxyl was not well defined so was not modeled in this structure. The extensive water network that is normally observed at the dimer interface in other GSTP1-1 structures is disrupted by binding of PAO. At occupancy of 0.6, the average temperature factor of the arsenic ions refined to 26 Å^2, similar to that of the C101 thiols (average of 28 Å^2). The arsenic ions form a 2.6 Å arsenic-sulfur bond with the thiol of C101 and are also within 3.0 Å of the carboxylate group of the glycyl moiety of GSH2 [Fig. 2].

This article is protected by copyright. All rights reserved.

Accepted Article

Binding of PAO to GSTP1-1 in the absence of GSH

In stressed cells the levels of GSH can be very low so we examined how GSTP1-1 interacts with PAO at low GSH concentrations. Binding of PAO to GSTP1-1 was followed on the basis of the quenching of intrinsic fluorescence of the protein [Fig. 1(B)]. Interestingly, the isothermic binding is strongly cooperative with an Hill coefficient of 1.85 and a $[PAO]_{0.5}$ = 28 μM (Table 1). We also evaluated the possible involvement of C47 or C101 on the binding of PAO. After replacing each of these residues separately with serine, the protein was still found to bind to PAO in a strongly cooperative process (n_H = 1.87) (Table 1) with $[PAO]_{0.5}$ values close to that found for the wild-type protein, being 8 μM and 15 μM for the C47S and C101S mutants, respectively. However, as expected, the double mutant C47S/C101S does not bind to the compound up to 0.1 M concentration.

Mass spectrometry reveals major and minor metalloid binding sites in the PAO only complex

In the absence of GSH several reaction products were observed, with one major species showing an increase in the deconvoluted mass of approximately 167 Da. This mass would be consistent with one phenylhydroxy-arsene-Cys complex per monomer. A minor species of 334 Da per monomer was observed and corresponds to two phenylhydroxy-arsene-Cys complexes per monomer. The kinetic (see above) and crystallographic studies (see below) are consistent with the major site of PAO reaction being at C47 and the minor site at C101. C47 has been shown previously to be the most reactive cysteine in apo GSTP1-1.[31]

Crystal structure of the GSTP1-1 PAO complex in the absence of GSH reveals metalloid binding at the dimer interface and displacement of helix α2

In the absence of GSH, electron density for the arsenic adduct is evident at the dimer interface, albeit at a low occupancy, bound to the thiol of C101 of each subunit [Fig. 3(A)]. The arsenic atoms refined to occupancies of 0.3 with an average temperature factor of 36

This article is protected by copyright. All rights reserved.

Accepted Article

Å^2, close to those of the C101 thiols (average of 38 Å^2). Interestingly, these sites are on the opposite side of the C101 thiols than that seen for the same peaks in the structure with GSH described above [Fig. 3(A,B)]. No electron density was evident for the phenyl ring or the hydroxy ligand, so they were excluded from refinement. The usual water network observed at the dimer interface in other GSTP1-1 structures is severely disrupted by binding of PAO, as was observed in the GSH-bound structure.

Strikingly, there is no electron density for the region corresponding to helix α2, (residues 35-50) suggesting it has become highly mobile and possibly disordered [Fig. 2(A,C)]. This region includes C47 and the kinetic studies showed that PAO reacts with this residue in the absence of GSH. In contrast, the same region in the GSH-bound structure described above is well ordered, consistent with published kinetic studies that C47 becomes inaccessible in the presence of GSH.[31] Thus we assume the absence of density in this region is a consequence of the G-site being empty and PAO binding to C47.

The C-terminal end of helix α2 includes Tyr49, a residue that has been described as a "key" that fits into a hydrophobic pocket (the "lock") of residues contributed from the neighboring subunit [Fig. 2(A)].[32] Mutational studies of Tyr49 show that it is a critical residue for stability of the GSTP1-1 dimer.[34] We visualize for the first time the consequences of removing the "key" from the "lock": the cleft at the dimer interface has widened markedly with an increase in the separation at the tip of the helical towers of ~8 Å. Superposition of the individual monomers onto the corresponding monomers in the GSH-bound structure described above indicates no significant changes in the monomeric structures (r.m.s.d. of ~0.3 Å). Superposition of one monomer of the PAO complex onto the published wild-type GSTP1-1 GSH complex structure (PDB id: 5GSS[33]) reveals a rotation of approximately 10º of the second monomer with respect to the first, pivoting at the base of the helical tower [Fig. 3(D)]. Superposition of the GSH-bound and GSH-absent dimers reveals that while the residues at the base of the dimer superimpose closely, the upper half of the dimer has separated. The distance between the C101 carbon alpha atoms

This article is protected by copyright. All rights reserved.

Accepted Article

has increased from 7.8 Å in the GSH-bound structure to 11.2 Å in the GSH-free structure. We confirmed this observation by collecting a further 3 data sets, each from one crystal, of the GSH-free PAO complex and the widening of the dimer interface to the same degree was consistent throughout.

Crystal structure of the GSTP1-1 PAO complex from crystals grown in the absence of GSH and subsequently soaked in GSH

To determine if binding of GSH to the active site was sufficient to re-stabilize helix α2, which forms one wall of the G-site, we took a PAO soaked crystal, in the absence of GSH, after two days, and reintroduced GSH. This crystal was from the same drop as the crystal used for the PAO structure described above. To our surprise, back-soaking this crystal in GSH for 5 days restored the structure of the disordered helix, including the 'lock-and-key' and re-stabilized the interaction between the monomers, resulting in a distance between the tips of the helical towers identical to that observed in published GSTP1-1 structures. C47 and C101 are no longer modified, presumably because the excess GSH competed with PAO at that site. Further, many of the critical waters that are usually observed in the dimer interface of other GSTP1-1 structures are again observed. This back-soaked structure has the di-GSH-phenyl arsenic species bound at each active site, each with an occupancy of 0.6 and average temperature factor of 25 $Å^2$.

Crystal structure of apo GSTP1-1

We next wanted to explore whether the absence of helix α2 and the widened interface were due to the absence of ligand in the G-site as such ligands are thought to stabilize the helix which forms one wall of the site. Although apo GSTP1-1 structures have previously been reported they were generated from crystals that were soaked in ligands that were not visible in the electron density maps. As it is possible that the ligands were still bound but disordered, we decided to solve an apo GSTP1-1 structure from crystals that were not

This article is protected by copyright. All rights reserved.

Accepted Article

soaked in any ligand. The structure shows good electron density for all regions of the protein, including helix α2 and the lock-and-key, and there is an extensive network of waters visible at the dimer interface and in the active sites. Although helix 2 can be observed, an analysis of temperature factors shows this region in both monomers is one of the most mobile regions in the structure in accord with published solution studies.[35-37] The V-shaped dimer cleft resembles that seen in published GSTP1-1 structures. Thus the disappearance of helix α2 and the widened cleft seen in the PAO complex is not due to absence of ligand in the active site.

EXAFS studies reveal that PAO binding to GSTP1-1 in the absence of GSH results in the formation of two As-S bonds

We undertook X-ray Absorption Spectroscopy (XAS) studies to determine the ligand environment of the arsenic binding sites in the enzyme. This study could only be done in the absence of GSH since PAO reacts with GSH rapidly in solution. Our crystallographic, mass spectrometry and kinetic studies, performed in parallel with the XAS studies, revealed that PAO could react with two sites (C47 and C101) on the enzyme. X-ray absorption near edge spectroscopic (XANES) data [Fig. 4(A)] showed that the oxidation state of arsenic remains as As(III) when PAO is bound to the enzyme. The white line peak energy was found to be identical to that of aqueous $As(GS)_3$, but a comparatively lower peak intensity indicated a lower symmetry environment, consistent with a 2S,1C coordination shell.[38]

Curve fitting analysis of extended X-ray absorption fine structure data (EXAFS) showed that arsenic was bound to two sulfur donor ligands at a bond distance of 2.24 Å in the GST-PAO complex (Table S1), with a model containing three As-S sulfur interactions producing a significantly greater fit error. Attempts to include an As-C fit component were complicated by strong EXAFS cancellation over the full data range with the longer distance As-S component, producing a characteristic minimum in the EXAFS Fourier

This article is protected by copyright. All rights reserved.

Accepted Article

transform at ~2 Å [Fig. 4(B)]. Nonetheless, a fit which included a fixed Debye-Waller factor for the As-C component produced an As-C bond distance of 1.93 Å which is consistent the median distance (1.96 Å) for such a bond in the eighty examples of similar coordination environments (2S,1C-phenyl) found in the Cambridge crystallographic database.

The EXAFS data are consistent with PAO forming a crosslink between C47 and C101. Inspection of the structure suggests the crosslink is most likely between monomers and the location of the arsenic anomalous signal on the opposite side of C101 to that observed in PAO GSH complex also supports this interpretation [Fig. 3(A-C)].

Discussion

PAO is considered a promising agent for treating certain types of leukemia and solid tumors that are resistant to other anti-cancer drugs, with an analog currently in human clinical trials.[30] However, in cancer cells PAO is readily attacked by GSH and protein thiols such as those in GSTP1-1, a detoxifying enzyme that is overexpressed in many types of cancer cells at millimolar concentrations.[1,2] Studies in yeast suggest that arsenic is mainly protein-bound in acute exposure situations whereas it is mainly GSH-bound after long-term exposure.[39] Thus GSTP1-1 may be a major cause of arsenic drug inactivation in human cancer cells. We show here that the GSH adduct of PAO is a potent inhibitor of GSTP1-1 with a K_i of 90 nM. We further show that the parent molecule, PAO, can react with C47 and C101 of the enzyme (Table 1).

The crystal structure of GSTP1-1 complexed to PAO, in the presence of GSH, reveals four arsenic ligands bind to the enzyme, connected to each other via an extensive network of interactions [Fig. 2(A)]. Bond lengths between the arsenic atom and the GSH thiol atoms are ~2.4 Å, which is in accordance with the expected bond lengths for this interaction.[40] This structure is very similar to the published wild-type GSH complex structure (PDB id: 5GSS[33]) with a r.m.s deviation in carbon alpha positions of 0.3 Å for

This article is protected by copyright. All rights reserved.

Accepted Article

414 residues. Despite the accommodation of an additional GSH ligand, as well as the phenyl-arsenic moiety in the active site, no significant movements are observed for any of the active site residues.

In the absence of GSH, the crystal structure shows that PAO binds to the C101 ligands at the dimer interface with an arsenic-sulfur bond distance of 2.4 Å [Fig. 3(A)]. The enzyme appears less reactive with PAO in the absence of GSH, suggesting that the GSH-mediated interactions with the arsenic-bound C101, observed in the PAO GSH complex, might facilitate and stabilize binding of arsenic at this site. Although C47 is not observed in the crystal structure our kinetic and mass spectrometry studies are consistent with PAO binding at this residue also. Mass spectrometry revealed a major reaction species in the absence of GSH that corresponds to one PAO per GST monomer and a second reaction species in the sample with two PAO per GST monomer. The crystallography data are consistent with C47 being the major site of PAO binding. EXAFS showed that arsenic was bound to two sulfur donor atoms at 2.2 Å and one carbon at 1.9 Å when PAO was incubated with GST in the absence of GSH [Fig. 4], indicating that the reaction resulted in the loss of the oxido ligand from PAO, but the retention of the phenyl group. Taken together the data support an intermonomer crosslink between C47 and C101 [Fig. 3(C)].

The most remarkable feature of the GSH-free PAO complex structure is the increase in width of the water-filled cleft at the dimer interface. Normally the distance between the alpha carbon atoms of residue 113, located at the top of the helical towers, is 22.3 Å but in the GSH-free PAO complex structure this distance is 28.2 Å [Fig. 3(D)].[33] The change in the dimer interface appears specific for PAO as the ligand was introduced by soaking pre-formed GST crystals using the same protocol that has been employed previously for numerous other GST ligands, none of which resulted in a change to the dimer interface.[33,41-45] Furthermore, the effect appears to be associated with PAO binding of C47 as binding at C101 in the presence of GSH did not cause any change to the dimer

This article is protected by copyright. All rights reserved.

Accepted Article

interface. This movement at the dimer interface is probably the cause of the strong cooperativity observed during PAO binding either to wild-type or to the single Cys mutants. This homotropic cooperative interaction, mimics the one produced by 6-(7-Nitro-2,1,3-benzoxadiazol-4-ylthio)hexanol when it binds to GSTP1-1 in the absence of GSH[46] and is likely made possible by the lock-and-key motif present at the dimer interface.[34]

A surprising feature of the GSH-free PAO complex is the absence of electron density for helix α2 (residues 35-50). Previously published "apo" human GSTP1-1 structures were derived from wild-type crystals soaked in ligands expected to bind in the active site giving rise to the doubt that the G-site was truly empty. Thus we decided to determine a new apo structure that revealed an intact helix α2. It thus seems likely that the disorder of helix α2 is associated with chemical modification of C47, which is known to be accessible only in the apoezyme.[31] Disruption of helix α2 by C47 modification with the more bulky PAO leads to withdrawal of the "key" residue, Tyr49, from its hydrophobic "lock" and subsequent weakening of the dimer interface. Others have shown that mutation of Tyr49 to alanine leads to unstable GST dimers.[34] Remarkably, the major disruptions caused to the GST structure could be reversed by back soaking GSH into crystals that were previously treated with PAO only.

The arsenic-based complexes presented here highlight the necessity to design and develop a novel drug that inhibits the enzyme at both the active site and the dimer interface to be as effective and optimal as possible. The GSTP1-1 PAO GSH structure described here provides a framework for the design of such compounds.

Accepted Article

This article is protected by copyright. All rights reserved.

Materials and Methods

Materials

Wild-type GSTP1-1 and mutants were expressed in *E. coli* and purified as described previously.[47]

Stability of PA(GS)2 complex and kinetic studies with GSTP1-1

The instability constant $K_{inst} = \frac{[GSH]^2[PAO]}{[PA(GS)_2]}$ was calculated by adding step-by-step GSH to a fixed concentration of PAO (60 μM) in potassium phosphate buffer 0.1 M pH 6.5 and recording absorbance at 273 nm to quantify the amount of the formed complex. Inhibition experiments of $PA(GS)_2$ on GSTP1-1 were performed by incubating 1 μg of enzyme in 0.1 M potassium phosphate buffer pH 6.5 (25°C) with variable amounts of GSH at fixed 1 mM CDNB at three different fixed $PA(GS)_2$ concentrations. Reaction rates were recorded at 340 nm.

Fluorescence study

The quenching of intrinsic fluorescence of enzyme (excitation wavelength 295 nm, emission wavelength 344 nm) was measured in a single photon counting spectrofluorometer Fluoromax-4 Horiba, after the addition of variable amounts of PAO and enzyme.

Crystallization

GSTP1-1 was expressed, purified and crystallized as described previously.[44] Co-crystallization experiments were not attempted because DTT, an essential ingredient for crystallization, would react with PAO. (GST P1-1 crystals only grow in reducing conditions, likely due to the two highly reactive surface cysteines in each monomer of the GST dimer). PAO (Sigma-Aldrich) was dissolved in DMSO to make a 20 mM stock solution. Aliquots of the stock were added to a reservoir solution and diluted to a final

This article is protected by copyright. All rights reserved.

Accepted Article

concentration of 0.2 – 2.0 mM PAO. Crystals were transferred to 2 µl drops and left to soak for periods of several hours to a week.

Structure determination

Unless otherwise stated all data sets were processed with MOSFLM[48] and scaled with the program SCALA.[49] The structures were solved by molecular replacement using PHASER[50] with a model of GSTP1-1 complexed to GSH (PDB id: 5GSS) as a probe. Model building was done with COOT,[51] interspersed by rounds of positional and isotropically restrained B-factor refinement using Phenix Refine.[52] A summary of the data collection and refinement statistics and molprobity[53] analysis for all structures, including their quality relative to other structures at similar resolutions, is provided in Table S2.

XAS studies

Results from the mass spectrometry suggested that interaction of PAO with the protein at a single site per monomer was optimal at 2:1 ratio of PAO for 10 hrs. XAS data were recorded at 20 K on beamline 20B at the Photon Factory (Tsukuba, Japan). K-edge As XAS were measured in fluorescence detection mode using a 36-element Ge monolithic pixel array detector (Eurisys).

Mass spectrometry studies

Reaction mixtures were analyzed by electrospray mass spectrometry on an Agilent 6510 Q-TOF LC/MS (Bio21 Institute, Melbourne University).

Statistical analysis

All experiments were performed in triplicate (i.e. on three distinct samples). Errors are given as SEM. Kinetics and spectroscopic data were analyzed by GraphPad Prism software (La Jolla, CA).

This article is protected by copyright. All rights reserved.

Accepted Article

Accepted Article

Accession numbers

The models have been deposited in the Protein Data Bank (http://www.rcsb.org/pdb/) under the accession numbers 5DCG (apo GSTP1-1), 5DAL (PAO GSH complex), 5DAK (PAO complex, no GSH) and 5DDL (PAO complex soaked into crystals and back-soaked with GSH).

SUPPLEMENTAL MATERIAL

Supplemental Material includes Supplemental Experimental Procedures, one figure and two tables.

ACKNOWLEDGMENTS

We thank Tilman Schmachtel and Volker Ullrich for suggesting to us that GSTP1-1 might bind PAO and encouraging us to pursue these studies. We thank Mike Gorman and Guido Hansen for advice and encouragement and Nancy Hancock for protein production. We also thank the BioCARS staff at the Advanced Photon Source and the staff at the Australian Synchrotron for their help. This work was supported by the Australian Synchrotron Research Program, which was funded by the Commonwealth of Australia under the Major National Research Facilities Program. Use of the Advanced Photon Source was supported by the U.S. DOE, Basic Energy Sciences, Office of Energy Research. This research was partly undertaken on the MX1 and MX2 beamlines at the Australian Synchrotron, Victoria, Australia. The XAS was undertaken at the Australian National Beamline Facility at the Photon Factory in Japan, operated by the Australian Synchrotron. We acknowledge the Australian Research Council for financial support and the High Energy Accelerator Research Organization (KEK) in Tsukuba, Japan, for operations support. This work was supported by grants from the Australian Research Council (ARC), the Australian Cancer Research Foundation to M.W.P., the Victorian Government Operational Infrastructure

This article is protected by copyright. All rights reserved.

Support Scheme to St. Vincent's Institute and from MIUR and Genesys SpA to M.L.B. L.J.P was supported by National Health and Medical Research Council of Australia (NHMRC) Dora Lush Scholarship and International Centre for Diffraction Data Crystallography Scholarship. D.B.A. was supported by an Australian Postgraduate Award and St Vincent's Foundation Scholarship. L.J.P and D.B.A. are now NHMRC C.J. Martin Fellows and M.W.P. is NHMRC Research Fellow.

Accepted Article

This article is protected by copyright. All rights reserved.

REFERENCES

1. Sheehan D, Meade G, Foley VM, Dowd CA (2001) Structure, function and evolution of glutathione transferases: implications for classification of non-mammalian members of an ancient enzyme superfamily. Biochem J 360:1-16.
2. Hayes JD, Flanagan JU, Jowsey IR (2005) Glutathione transferases. Annu Rev Pharmacol Toxicol 45:51-88.
3. Mannervik B, Castro VM, Danielson UH, Tahir MK, Hansson J, Ringborg U (1987) Expression of class Pi glutathione transferase in human malignant melanoma cells. Carcinogenesis 8:1929-1932.
4. Townsend DM, Tew KD (2003) The role of glutathione-S-transferase in anti-cancer drug resistance. Oncogene 22:7369-7375.
5. Gallagher RE (1998) Arsenic--new life for an old potion. N Engl J Med 339:1389-1391.
6. Larson RA, Kondo K, Vardiman JW, Butler AE, Golomb HM, Rowley JD (1984) Evidence for a 15;17 translocation in every patient with acute promyelocytic leukemia. Am J Med 76:827-841.
7. Kwong YL, Todd D (1997) Delicious poison: arsenic trioxide for the treatment of leukemia. Blood 89:3487-3488.
8. Bradley D (2000) Therapeutic needs revive arsenic compound. Pharm Sci Technolo Today 3:401.
9. Murgo AJ (2001) Clinical trials of arsenic trioxide in hematologic and solid tumors: overview of the National Cancer Institute Cooperative Research and Development Studies. Oncologist 6 Suppl 2:22-28.
10. Bahlis NJ, McCafferty-Grad J, Jordan-McMurry I, Neil J, Reis I, Kharfan-Dabaja M, Eckman J, Goodman M, Fernandez HF, Boise LH et al (2002) Feasibility and correlates of arsenic trioxide combined with ascorbic acid-mediated depletion of

Accepted Article

This article is protected by copyright. All rights reserved.

intracellular glutathione for the treatment of relapsed/refractory multiple myeloma. Clin Cancer Res 8:3658-3668.

11. Akao Y, Yamada H, Nakagawa Y (2000) Arsenic-induced apoptosis in malignant cells in vitro. Leuk Lymphoma 37:53-63.
12. Zhang TC, Cao EH, Li JF, Ma W, Qin JF (1999) Induction of apoptosis and inhibition of human gastric cancer MGC-803 cell growth by arsenic trioxide. Eur J Cancer 35:1258-1263.
13. Woo SH, Park IC, Park MJ, Lee HC, Lee SJ, Chun YJ, Lee SH, Hong SI, Rhee CH (2002) Arsenic trioxide induces apoptosis through a reactive oxygen species-dependent pathway and loss of mitochondrial membrane potential in HeLa cells. Int J Oncol 21:57-63.
14. Lee TC, Wei ML, Chang WJ, Ho IC, Lo JF, Jan KY, Huang H (1989) Elevation of glutathione levels and glutathione S-transferase activity in arsenic-resistant Chinese hamster ovary cells. In Vitro Cell Dev Biol 25:442-448.
15. Wang Z, Dey S, Rosen BP, Rossman TG (1996) Efflux-mediated resistance to arsenicals in arsenic-resistant and -hypersensitive Chinese hamster cells. Toxicol Appl Pharmacol 137:112-119.
16. Romach EH, Zhao CQ, Del Razo LM, Cebrian ME, Waalkes MP (2000) Studies on the mechanisms of arsenic-induced self tolerance developed in liver epithelial cells through continuous low-level arsenite exposure. Toxicol Sci 54:500-508.
17. Lo JF, Wang HF, Tam MF, Lee TC (1992) Glutathione S-transferase pi in an arsenic-resistant Chinese hamster ovary cell line. Biochem J 288 (Pt 3):977-982.
18. Wang HF, Lee TC (1993) Glutathione S-transferase pi facilitates the excretion of arsenic from arsenic-resistant Chinese hamster ovary cells. Biochem Biophys Res Commun 192:1093-1099.
19. Liu J, Chen H, Miller DS, Saavedra JE, Keefer LK, Johnson DR, Klaassen CD, Waalkes MP (2001) Overexpression of glutathione S-transferase II and multidrug

This article is protected by copyright. All rights reserved.

Accepted Article

resistance transport proteins is associated with acquired tolerance to inorganic arsenic. Mol Pharmacol 60:302-309.

20. Jing Y, Dai J, Chalmers-Redman RM, Tatton WG, Waxman S (1999) Arsenic trioxide selectively induces acute promyelocytic leukemia cell apoptosis via a hydrogen peroxide-dependent pathway. Blood 94:2102-2111.

21. Lu M, Xia L, Luo D, Waxman S, Jing Y (2004) Dual effects of glutathione-S-transferase pi on As2O3 action in prostate cancer cells: enhancement of growth inhibition and inhibition of apoptosis. Oncogene 23:3945-3952.

22. Zhou L, Jing Y, Styblo M, Chen Z, Waxman S (2005) Glutathione-S-transferase pi inhibits As2O3-induced apoptosis in lymphoma cells: involvement of hydrogen peroxide catabolism. Blood 105:1198-1203.

23. Kitchin KT (2001) Recent advances in arsenic carcinogenesis: modes of action, animal model systems, and methylated arsenic metabolites. Toxicol Appl Pharmacol 172:249-261.

24. Xie Y, Liu J, Liu Y, Klaassen CD, Waalkes MP (2004) Toxicokinetic and genomic analysis of chronic arsenic exposure in multidrug-resistance mdr1a/1b(-/-) double knockout mice. Mol Cell Biochem 255:11-18.

25. Leslie EM, Haimeur A, Waalkes MP (2004) Arsenic transport by the human multidrug resistance protein 1 (MRP1/ABCC1). Evidence that a tri-glutathione conjugate is required. J Biol Chem 279:32700-32708.

26. Oetken C, von Willebrand M, Marie-Cardine A, Pessa-Morikawa T, Stahls A, Fisher S, Mustelin T (1994) Induction of hyperphosphorylation and activation of the p56lck protein tyrosine kinase by phenylarsine oxide, a phosphotyrosine phosphatase inhibitor. Mol Immunol 31:1295-1302.

27. Estrov Z, Manna SK, Harris D, Van Q, Estey EH, Kantarjian HM, Talpaz M, Aggarwal BB (1999) Phenylarsine oxide blocks interleukin-1beta-induced

Accepted Article

This article is protected by copyright. All rights reserved.

activation of the nuclear transcription factor NF-kappaB, inhibits proliferation, and induces apoptosis of acute myelogenous leukemia cells. Blood 94:2844-2853.

28. Larochette N, Decaudin D, Jacotot E, Brenner C, Marzo I, Susin SA, Zamzami N, Xie Z, Reed J, Kroemer G (1999) Arsenite induces apoptosis via a direct effect on the mitochondrial permeability transition pore. Exp Cell Res 249:413-421.

29. Sahara N, Takeshita A, Kobayashi M, Shigeno K, Nakamura S, Shinjo K, Naito K, Maekawa M, Horii T, Ohnishi K and others (2004) Phenylarsine oxide (PAO) more intensely induces apoptosis in acute promyelocytic leukemia and As2O3-resistant APL cell lines than As2O3 by activating the mitochondrial pathway. Leuk Lymphoma 45:987-995.

30. Horsley L, Cummings J, Middleton M, Ward T, Backen A, Clamp A, Dawson M, Farmer H, Fisher N, Halbert G and others (2013) A phase 1 trial of intravenous 4-(N-(S-glutathionylacetyl)amino) phenylarsenoxide (GSAO) in patients with advanced solid tumours. Cancer Chemother Pharmacol 72:1343-1352.

31. Ricci G, Lo Bello M, Caccurri AM, Pastore A, Nuccetelli M, Parker MW, Federici G (1995) Site-directed mutagenesis of human glutathione transferase P1-1. Mutation of Cys-47 induces a positive cooperativity in glutathione transferase P1-1. J Biol Chem 270:1243-1248.

32. Wilce MC, Parker MW (1994) Structure and function of glutathione S-transferases. Biochim Biophys Acta 1205:1-18.

33. Oakley AJ, Lo Bello M, Battistoni A, Ricci G, Rossjohn J, Villar HO, Parker MW (1997) The structures of human glutathione transferase P1-1 in complex with glutathione and various inhibitors at high resolution. J Mol Biol 274:84-100.

34. Hegazy UM, Mannervik B, Stenberg G (2004) Functional role of the lock and key motif at the subunit interface of glutathione transferase p1-1. J Biol Chem 279:9586-9596.

Accepted Article

This article is protected by copyright. All rights reserved.

Accepted Article

35. Ricci G, Caccuri AM, Lo Bello M, Rosato N, Mei G, Nicotra M, Chiessi E, Mazzetti AP, Federici G (1996) Structural flexibility modulates the activity of human glutathione transferase P1-1. Role of helix 2 flexibility in the catalytic mechanism. J Biol Chem 271:16187-16192.

36. Hitchens TK, Mannervik B, Rule GS (2001) Disorder-to-order transition of the active site of human class Pi glutathione transferase, GST P1-1. Biochemistry 40:11660-11669.

37. Stella L, Caccuri AM, Rosato N, Nicotra M, Lo Bello M, De Matteis F, Mazzetti AP, Federici G, Ricci G (1998) Flexibility of helix 2 in the human glutathione transferase P1-1. time-resolved fluorescence spectroscopy. J Biol Chem 273:23267-23273.

38. Munro KL, Mariana A, Klavins AI, Foster AJ, Lai B, Vogt S, Cai Z, Harris HH, Dillon CT (2008) Microprobe XRF mapping and XAS investigations of the intracellular metabolism of arsenic for understanding arsenic-induced toxicity. Chem Res Toxicol 21:1760-1769.

39. Talemi SR, Jacobson T, Garla V, Navarrete C, Wagner A, Tamas MJ, Schaber J (2014) Mathematical modelling of arsenic transport, distribution and detoxification processes in yeast. Mol Microbiol 92:1343-1356.

40. Allen FH (2002) The Cambridge Structural Database: a quarter of a million crystal structures and rising. Acta Cryst B58:380-388.

41. Ang WH, Parker LJ, De Luca A, Juillerat-Jeanneret L, Morton CJ, Lo Bello M, Parker MW, Dyson PJ (2009) Rational design of an organometallic glutathione transferase inhibitor. Angew Chem Int Ed Engl 48:3854-3857.

42. Cesareo E, Parker LJ, Pedersen JZ, Nuccetelli M, Mazzetti AP, Pastore A, Federici G, Caccuri AM, Ricci G, Adams JJ and others (2005) Nitrosylation of human glutathione transferase P1-1 with dinitrosyl diglutathionyl iron complex in vitro and in vivo. J Biol Chem 280:42172-42180.

This article is protected by copyright. All rights reserved.

Accepted Article

43. Oakley AJ, Lo Bello M, Nuccetelli M, Mazzetti AP, Parker MW (1999) The ligandin (non-substrate) binding site of human Pi class glutathione transferase is located in the electrophile binding site (H-site). J Mol Biol 291:913-926.

44. Parker LJ, Ciccone S, Italiano LC, Primavera A, Oakley AJ, Morton CJ, Hancock NC, Bello ML, Parker MW (2008) The anti-cancer drug chlorambucil as a substrate for the human polymorphic enzyme glutathione transferase P1-1: kinetic properties and crystallographic characterisation of allelic variants. J Mol Biol 380:131-144.

45. Parker LJ, Italiano LC, Morton CJ, Hancock NC, Ascher DB, Aitken JB, Harris HH, Campomanes P, Rothlisberger U, De Luca A et al (2011) Studies of glutathione transferase P1-1 bound to a platinum(IV)-based anticancer compound reveal the molecular basis of its activation. Chemistry 17:7806-7816.

46. Ricci G, De Maria F, Antonini G, Turella P, Bullo A, Stella L, Filomeni G, Federici G, Caccuri AM (2005) 7-Nitro-2,1,3-benzoxadiazole derivatives, a new class of suicide inhibitors for glutathione S-transferases. Mechanism of action of potential anticancer drugs. J Biol Chem 280:26397-26405.

47. Lo Bello M, Battistoni A, Mazzetti AP, Board PG, Muramatsu M, Federici G, Ricci G (1995) Site-directed mutagenesis of human glutathione transferase P1-1. Spectral, kinetic, and structural properties of Cys-47 and Lys-54 mutants. J Biol Chem 270:1249-1253.

48. Leslie AW, Powell H. Processing diffraction data with mosflm. In: Read R, Sussman J, editors. Evolving Methods for Macromolecular Crystallography. Volume 245, NATO Science Series: Springer Netherlands; 2007. p 41-51.

49. Collaborative Computational Project N (1994) The CCP4 Suite: Programs for Protein Crystallography. Acta Cryst D50:760-763.

50. McCoy AJ, Grosse-Kunstleve RW, Adams PD, Winn MD, Storoni LC, Read RJ (2007) Phaser crystallographic software. J Appl Cryst 40:658-674.

This article is protected by copyright. All rights reserved.

51. Emsley P, Cowtan K (2004) Coot: model-building tools for molecular graphics. Acta Cryst D60:2126-2132.

52. Adams PD, Afonine PV, Bunkoczi G, Chen VB, Davis IW, Echols N, Headd JJ, Hung LW, Kapral GJ, Grosse-Kunstleve RW et al (2010) PHENIX: a comprehensive Python-based system for macromolecular structure solution. Acta Cryst D66:213-221.

53. Chen VB, Arendall WB, 3rd, Headd JJ, Keedy DA, Immormino RM, Kapral GJ, Murray LW, Richardson JS, Richardson DC (2010) MolProbity: all-atom structure validation for macromolecular crystallography. Acta Cryst D66:12-21.

Accepted Article

This article is protected by copyright. All rights reserved.

TABLES

Table 1 Kinetic data of PAO and $PA(GS)_2$ binding to GSTP1-1 wild-type and mutants

	K_m (M)	K_i (M)[a]	$[PAO]_{0.5}$ (M)[b]	n_H[b]
wt	$1.2 \pm 0.2 \times 10^{-4}$	$9 \pm 2 \times 10^{-8}$	$28 \pm 11 \times 10^{-6}$	1.8 ± 0.2
C47S	$1.3 \pm 0.3 \times 10^{-3}$	$3.0 \pm 0.3 \times 10^{-6}$	$8 \pm 3 \times 10^{-6}$	1.9 ± 0.4
C101S	$2.7 \pm 0.4 \times 10^{-4}$	$3.5 \pm 0.4 \times 10^{-7}$	$15 \pm 6 \times 10^{-6}$	1.9 ± 0.3
C47S/C101S	$2.1 \pm 0.4 \times 10^{-3}$	-	$> 10^{-4}$	-

Each experiment was performed in triplicate (i.e. three different spectrophotometric determinations on three distinct samples) and errors are SEM.

[a] K_i is the inhibition constant for the competitive inhibition of GSTP1-1 (wt and mutants) by $PA(GS)_2$ complex.

[b] $[PAO]_{0.5}$ i.e. the concentration of the inhibitor that causes 50% of the fluorescence quenching at saturation. n_H are calculated from quenching fluorescence experiments of GSTP1-1 (wt and mutants) and PAO.

Accepted Article

This article is protected by copyright. All rights reserved.

FIGURE LEGENDS

Figure 1. Kinetic studies of PAO binding to GSTP1-1. (A) UV absorption spectra of PA(GS)2 complex. 1 mM GSH was reacted with variable amounts of PAO 33 μM (—), 66 μM (----), 100 μM (−−−−) in 0.1 M potassium phosphate buffer, pH 6.5. The spectrum of PAO alone (100 μM) is also reported (−··−··−··). (B) Binding of PAO to GSTP1-1 was followed on the basis of the quenching of intrinsic fluorescence at 344 nm ($\lambda_{exc.}$ = 295 nm). GSTP1-1 (1 μM) was incubated with variable amounts of PA(GS)2 (from 3 to 60 μM) in 0.1 M potassium phosphate buffer, pH 6.5 (25°C). $[PAO]_{05}$ = 28 μM; n_H = 1.85. Experiment was performed in triplicate (i.e. three different spectrophotometric determinations performed on three distinct samples). Error bars represent SEM.

Figure 2. Crystal structure of the GSTP1-1 PAO GSH complex. (A) Ribbon representation of GSTP1-1 showing the network of interactions across the dimer interface. The arsenic atoms are shown as purple spheres, GSH and the phenyl ligands and the reactive cysteines as sticks with atomic coloring. The locations of helix α2, the reactive cysteines and the "key" residue Tyr 49 are also indicated. (B) Close-up view of the active site cleft, with the protein shown as a solvent-accessible surface and the GSH, arsenic and phenyl ligands shown as in panel *A*. (C) Stereoview of the final $2F_O$-F_C electron density map (contour level 1σ in blue) and anomalous difference Fourier maps (contour at 8σ in pink) of the diGSH-phenyl-arsenic complex bound in the active site of one chain in the GSTP1-1 dimer. Surrounding residues are shown as sticks and waters shown as red spheres. Putative hydrogen bonds between water molecules and the ligand are shown as yellow dashed lines, with direct bonding (intermolecular) interactions between the bound ligands and between the ligand and protein shown as grey dashed lines. Some key residues discussed in the text are labeled.

This article is protected by copyright. All rights reserved.

Accepted Article

Figure 3. Crystal structure of the GSTP1-1 PAO complex. (A), (B) Views of the final $2F_O$-F_C electron density map (contour level 1σ in blue) and anomalous difference Fourier maps (contour at 8σ in pink) of PAO bound to Cys101 at the dimer interface. In panel *A* the PAO complex structure is shown and in panel *B* the PAO GSH complex is shown by way of comparison. (C) Ribbon representation of GSTP1-1 suggesting how PAO is able to crosslink monomers via the reactive cysteines. The arsenic atoms are shown as purple spheres with Cys101 as sticks with atomic coloring. The disordered helix-α2 is represented by the dashed orange line for both chains of the GSTP1-1 dimer, with the putative position of the other reactive cysteine Cys47 represented diagrammatically as a bond to the arsenic. (D) Superposition of subunit A of the GTSP1-1 GSH complex (PDB id:5GSS) onto subunit A of the GSH-free PAO complex (ribbon depiction). The movements of subunit B of the GSH-free PAO complex (grey) with respect to the GSH-bound structure (purple) are depicted by alpha-carbon traces.

Figure 4. X-ray absorption spectroscopy of PAO binding to GSTP1-1. (A) As K-edge X-ray absorption near edge spectra for GST incubated with PAO in the absence of GSH (black trace), $As(GS)_{3(aq)}$ (red), aqueous arsenite (green) and aqueous arsenate (blue). Vertical lines are drawn at 11,870 and 11875 eV. (B) As K-edge EXAFS spectrum (left) and corresponding phase-corrected Fourier transform (right) of GST incubated with PAO in the absence of GSH. The calculated fit from model 1 in Supporting Information Table S1 is shown as the dotted trace in both k and R space.

Accepted Article

This article is protected by copyright. All rights reserved.

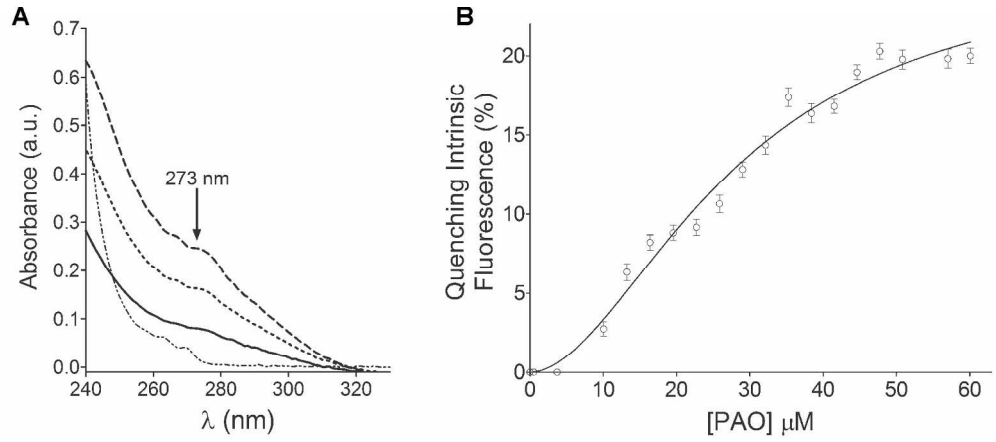

Figure 1. Kinetic studies of PAO binding to GSTP1-1. (A) UV absorption spectra of PA(GS)2 complex. 1 mM GSH was reacted with variable amounts of PAO 33 μM (____), 66 μM (- - - -), 100 μM (−−−−) in 0.1 M potassium phosphate buffer, pH 6.5. The spectrum of PAO alone (100 μM) is also reported (−··−··−··). (B) Binding of PAO to GSTP1-1 was followed on the basis of the quenching of intrinsic fluorescence at 344 nm (λexc. = 295 nm). GSTP1-1 (1 μM) was incubated with variable amounts of PA(GS)2 (from 3 to 60 μM) in 0.1 M potassium phosphate buffer, pH 6.5 (25 °C). [PAO]05 = 28 μM; nH = 1.85. Experiment was performed in triplicate (i.e. three different spectrophotometric determinations performed on three distinct samples). Error bars represent SEM.
Fig. 1
177x77mm (300 x 300 DPI)

Accepte

This article is protected by copyright. All rights reserved.

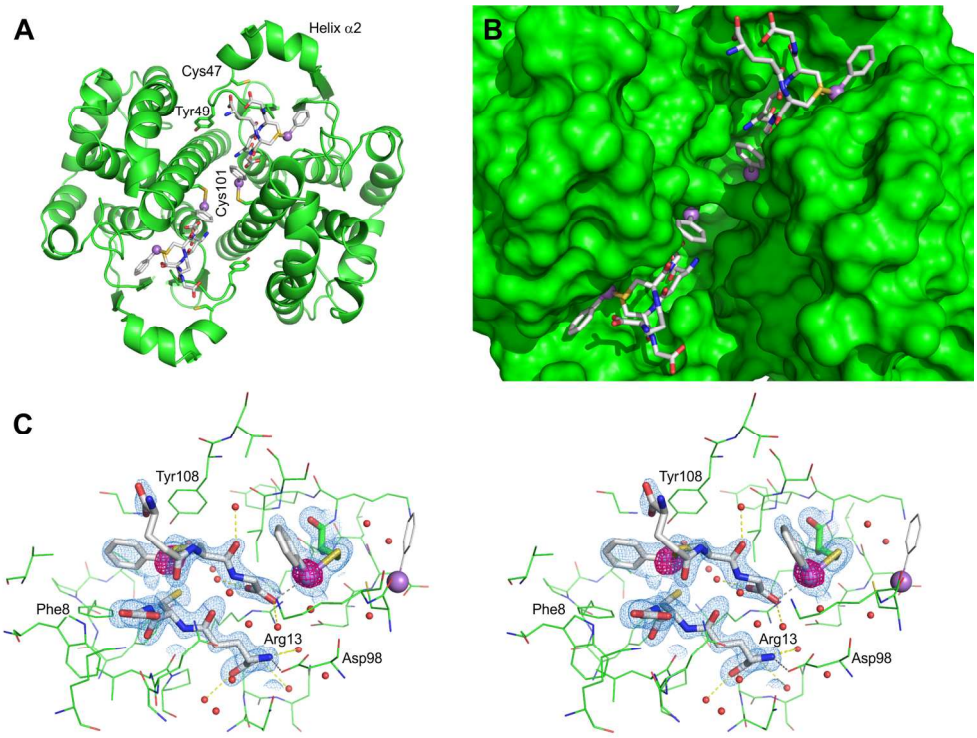

Figure 2. Crystal structure of the GSTP1-1 PAO GSH complex. (A) Ribbon representation of GSTP1-1 showing the network of interactions across the dimer interface. The arsenic atoms are shown as purple spheres, GSH and the phenyl ligands and the reactive cysteines as sticks with atomic coloring. The locations of helix α2, the reactive cysteines and the "key" residue Tyr 49 are also indicated. (B) Close-up view of the active site cleft, with the protein shown as a solvent-accessible surface and the GSH, arsenic and phenyl ligands shown as in panel A. (C) Stereoview of the final 2Fo-Fc electron density map (contour level 1σ in blue) and anomalous difference Fourier maps (contour at 8σ in pink) of the diGSH-phenyl-arsenic complex bound in the active site of one chain in the GSTP1-1 dimer. Surrounding residues are shown as sticks and waters shown as red spheres. Putative hydrogen bonds between water molecules and the ligand are shown as yellow dashed lines, with direct bonding (intermolecular) interactions between the bound ligands and between the ligand and protein shown as grey dashed lines. Some key residues discussed in the text are labeled.

Fig. 2

177x133mm (300 x 300 DPI)

Ac

This article is protected by copyright. All rights reserved.

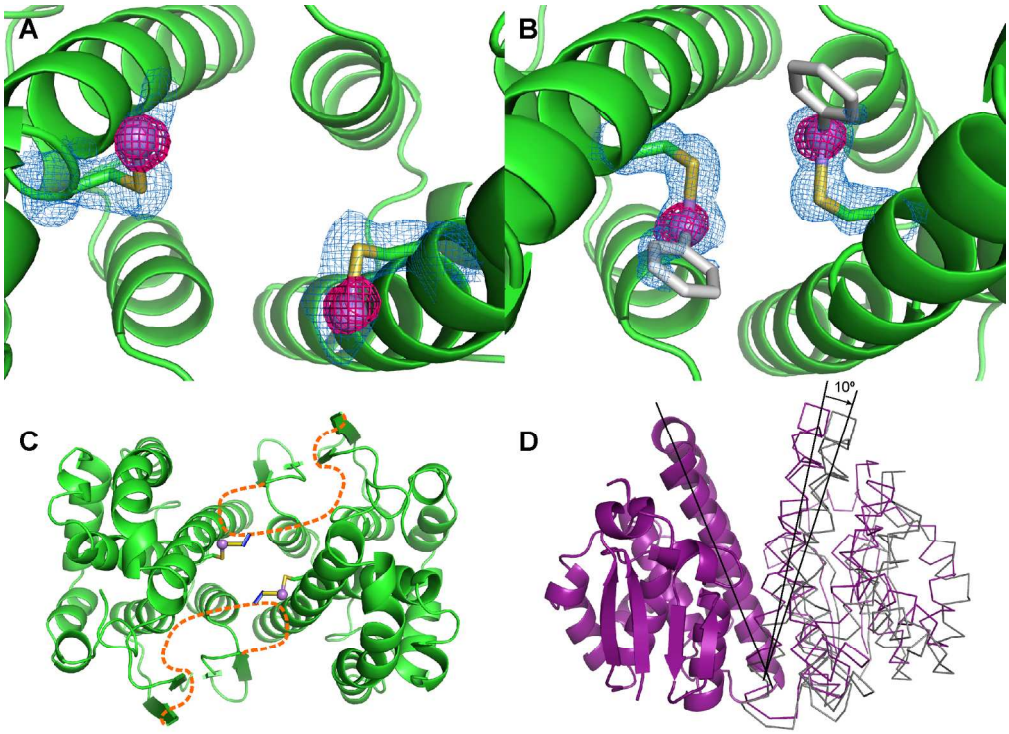

Figure 3. Crystal structure of the GSTP1-1 PAO complex. (A), (B) Views of the final 2Fo-Fc electron density map (contour level 1σ in blue) and anomalous difference Fourier maps (contour at 8σ in pink) of PAO bound to Cys101 at the dimer interface. In panel A the PAO complex structure is shown and in panel B the PAO GSH complex is shown by way of comparison. (C) Ribbon representation of GSTP1-1 suggesting how PAO is able to crosslink monomers via the reactive cysteines. The arsenic atoms are shown as purple spheres with Cys101 as sticks with atomic coloring. The disordered helix-α2 is represented by the dashed orange line for both chains of the GSTP1-1 dimer, with the putative position of the other reactive cysteine Cys47 represented diagrammatically as a bond to the arsenic. (D) Superposition of subunit A of the GTSP1-1 GSH complex (PDB id:5GSS) onto subunit A of the GSH-free PAO complex (ribbon depiction). The movements of subunit B of the GSH-free PAO complex (grey) with respect to the GSH-bound structure (purple) are depicted by alpha-carbon traces.

Fig. 3
177x133mm (300 x 300 DPI)

Ac

This article is protected by copyright. All rights reserved.

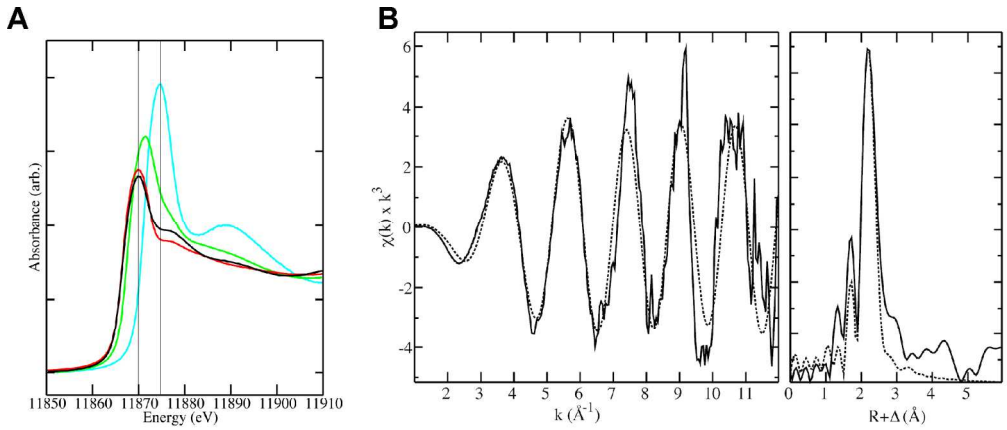

Figure 4. X-ray absorption spectroscopy of PAO binding to GSTP1-1. (A) As K-edge X-ray absorption near edge spectra for GST incubated with PAO in the absence of GSH (black trace), As(GS)3(aq) (red), aqueous arsenite (green) and aqueous arsenate (blue). Vertical lines are drawn at 11,870 and 11875 eV. (B) As K-edge EXAFS spectrum (left) and corresponding phase-corrected Fourier transform (right) of GST incubated with PAO in the absence of GSH. The calculated fit from model 1 in Supporting Information Table S1 is shown as the dotted trace in both k and R space.

Fig. 4

177x76mm (300 x 300 DPI)

Accepted

This article is protected by copyright. All rights reserved.

SUPPLEMENTARY MATERIAL

SUPPLEMENTAL TABLES

Table S1. Parameters fit to the EXAFS spectrum of the PAO GSTP1-1 complex in frozen solution[a]

Model	bond	coordination number (*N*)	interatomic distance (*R*, Å)	Debye-Waller factor (σ^2, Å^{-2})	$-\Delta E_0$ (eV)	fit error (%)
1	**As-S** **As-C**	**2** **1**	**2.243(4)** **1.93(1)**	**0.0025(2)** **0.0019[b]**	**10.4(8)**	**43.9**
2	As-S As-C	3 1	2.239(4) 1.903(9)	0.0053(3) 0.0019[b]	10.7(2)	44.9
3	As-S	2	2.258(4)	0.0030(1)	6.8(2)	48.7
4	As-S	3	2.251(4)	0.0057(2)	8.1(8)	50.6

[a]The *k*-range was 1 – 12 Å^{-1} for all fits. A scale factor (S_0^2) of 0.9 was used for all fits. $\Delta E_0 = E_0 - 11867$ eV where E_0 is the threshold energy. Values in parentheses are the estimated standard deviation derived from the diagonal elements of the covariance matrix and are a measure of precision. The fit-error is defined as $[\Sigma k^6(\chi_{exp}-\chi_{calc})^2/\Sigma k^6\chi_{exp}^2]^{½}$.

[b]This parameter was fixed in this model – an attempt to refine it resulted in a physically unreasonable value (i.e. < 0.001). Note that only the fit errors from either models 1 and 2, or models 3 and 4, can be directly compared, as the latter pair of models contains fewer fitted parameters.

John Wiley & Sons

This article is protected by copyright. All rights reserved.

Accepted Article

Table S2. Summary of data collection and structure refinement

Data Collection	PAO-GSH	PAO	GSH back-soaked	APO
X-ray source	BioCARS (APS)	MX1 (AS)	MX1 (AS)	In-house
Temperature (K)	100	100	100	100
Space group	*C2*	*C2*	*C2*	*C2*
Cell dimensions				
a (Å)	77.6	74.6	77.7	77.5
b (Å)	90.2	95.5	89.8	90.3
c (Å)	68.7	68.3	68.9	68.9
β (º)	98.0	98.3	98.1	98.5
GST protomers in asymmetric unit	2	2	2	2
Maximum resolution (Å)	1.5 (1.53-1.5)	2.1 (2.18-2.1)	1.98(2.03-1.98)	2.01 (2.06-2.01)
No. of crystals	1	1	1	1
No. of observations	508961 (26101)	811831 (61865)	488857 (30648)	149880 (10403)
No. of unique reflections	74367 (7397)	54535 (5026)	32553 (2232)	30673 (2217)
Data completeness (%)	99.5 (99.4)	98.3 (90.9)	99.9 (98.8)	98.0 (95.6)
R_{merge} [a]	7.6 (78.7)	10.3 (72.9)	6.1 (28.6)	11.6 (22.4)
I/σ_I	15.2 (2.1)	18.8 (3.5)	27 (7.4)	9.7 (5.7)
Multiplicity	6.8 (7.0)	14.9 (12.3)	15 (13.7)	4.9 (4.7)
Refinement				
Number of non-hydrogen atoms				
Protein	3289	3022	3270	3264
Arsenic complex	108	2	94	-
GSH	40	-	40	-
MES	24	24	24	24
SO_4^{2-}	5	-	5	-

Accepted Article

John Wiley & Sons

This article is protected by copyright. All rights reserved.

PO_4^{2-}	-	-	-	10
Ca^{2+}	-	-	2	1
Solvent (H_2O)	480	239	403	457
Resolution (Å)	1.5	2.1	2.0	2.0
R_{cryst}[b] (%)	18.0 (26.7)	15.7 (23.7)	14.1 (16.7)	14.6 (17.1)
R_{free}[c] (%)	21.3 (29.5)	20.4 (29.6)	17.2 (20.3)	18.3 (22.4)
Reflections used in R_{conv}				
Number	74359	50403	32552	30673
rmsd's from ideal geometry:				
Bonds (Å)	0.011	0.012	0.006	0.004
Angles (°)	1.4	1.4	1.1	0.9
Wilson B-factor	15.0	22.5	18.3	12.3
Mean B (Å^2)				
protein	19.9	25.2	15.8	13.8
solvent	29.6	30.3	23.2	21.6
ligands	25.4	40.5	23.6	28.1
PAO	33.3	-	-	-
GSH	20.9	-	18.7	-
$PAO(GS)_2$	27.1	-	24.6	-
As	-	36	-	-
Molprobity[d]				
clashscore	2	3	2	1
Ramachandran outliers (5)	0.2	0.8	0.2	0
side-chain outliers (%)	0.6	1.6	0.9	1.2
RSRZ outliers (%)	5.7	0.5	0.7	0

Accepted Article

John Wiley & Sons

This article is protected by copyright. All rights reserved.

The values in parentheses are for the highest resolution bin. BioCARS (APS) is the BioCARS beamline at the Advanced Photon Source, Chicago, USA. MX1 (AS) is the MX1 beamline at the Australian Synchrotron. In-house is the home X-ray source as described in Materials and Methods.

[a] $R_{merge} = \Sigma_{hkl}\Sigma_i|I_i - \langle I\rangle|/|\langle I\rangle|$, where I_i is the intensity for the ith measurement of an equivalent reflection with indices h,k,l.

[b] $R_{cryst} = \Sigma||F_{obs}| - |F_{calc}||/\Sigma|F_{obs}|$, where F_{obs} and F_{calc} are the observed and calculated structure factor amplitudes respectively.

[c] R_{free} was calculated with 5% of the diffraction data that were selected randomly and not used throughout refinement.

[d] Molprobity [1] output statistics of deposited model.

Accepted Article

John Wiley & Sons

This article is protected by copyright. All rights reserved.

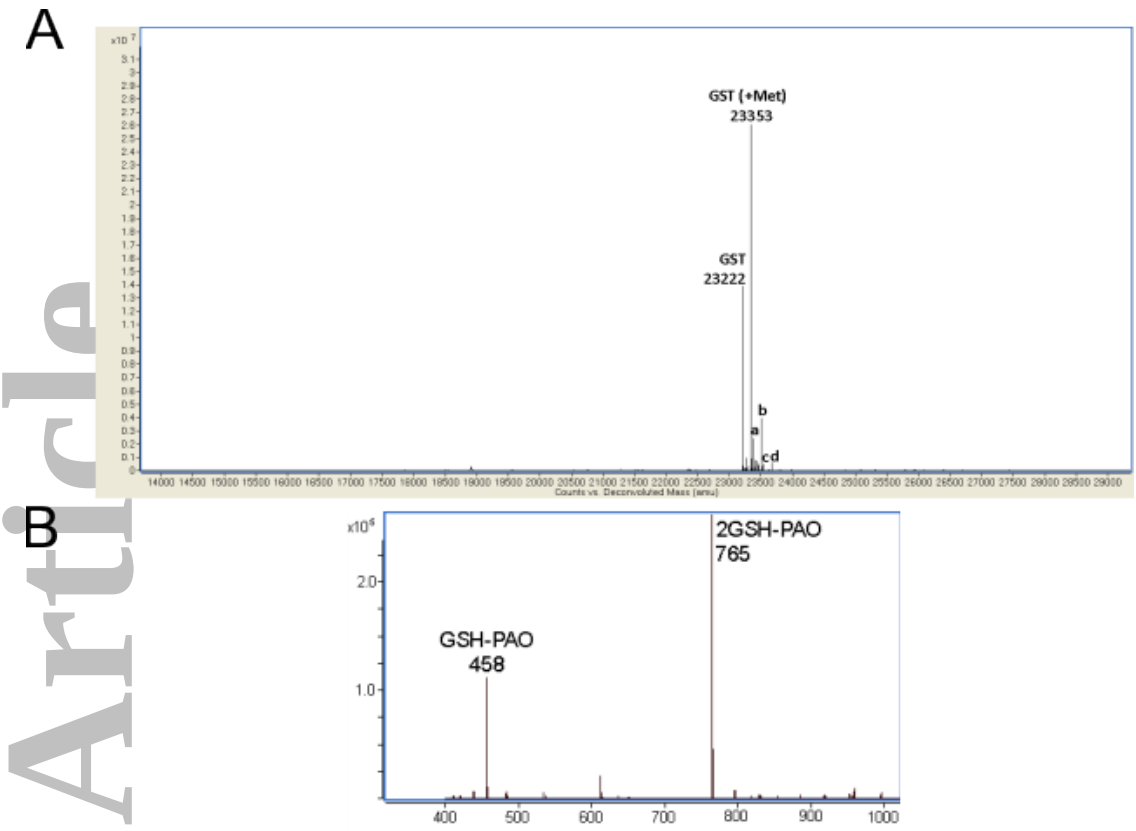

Figure S1. Mass spectroscopic analysis of samples containing PAO showing products formed through reaction. (A) Products formed during reaction of GSTP1-1 with PAO in the absence of GSH. Peaks are **a**: GST+PAO, **b**: GST-Met+PAO, **c**: GST+2xPAO and **d**: GST-Met+2xPAO. (Met is N-terminal methionine which is typically present in ~50% of protein sample). (B) Products formed during reaction of GSTP1-1 with PAO in the presence of GSH. No GSTP1-1 conjugates form as the GSH preferentially reacts with the PAO.

Accepted Article

John Wiley & Sons

This article is protected by copyright. All rights reserved.

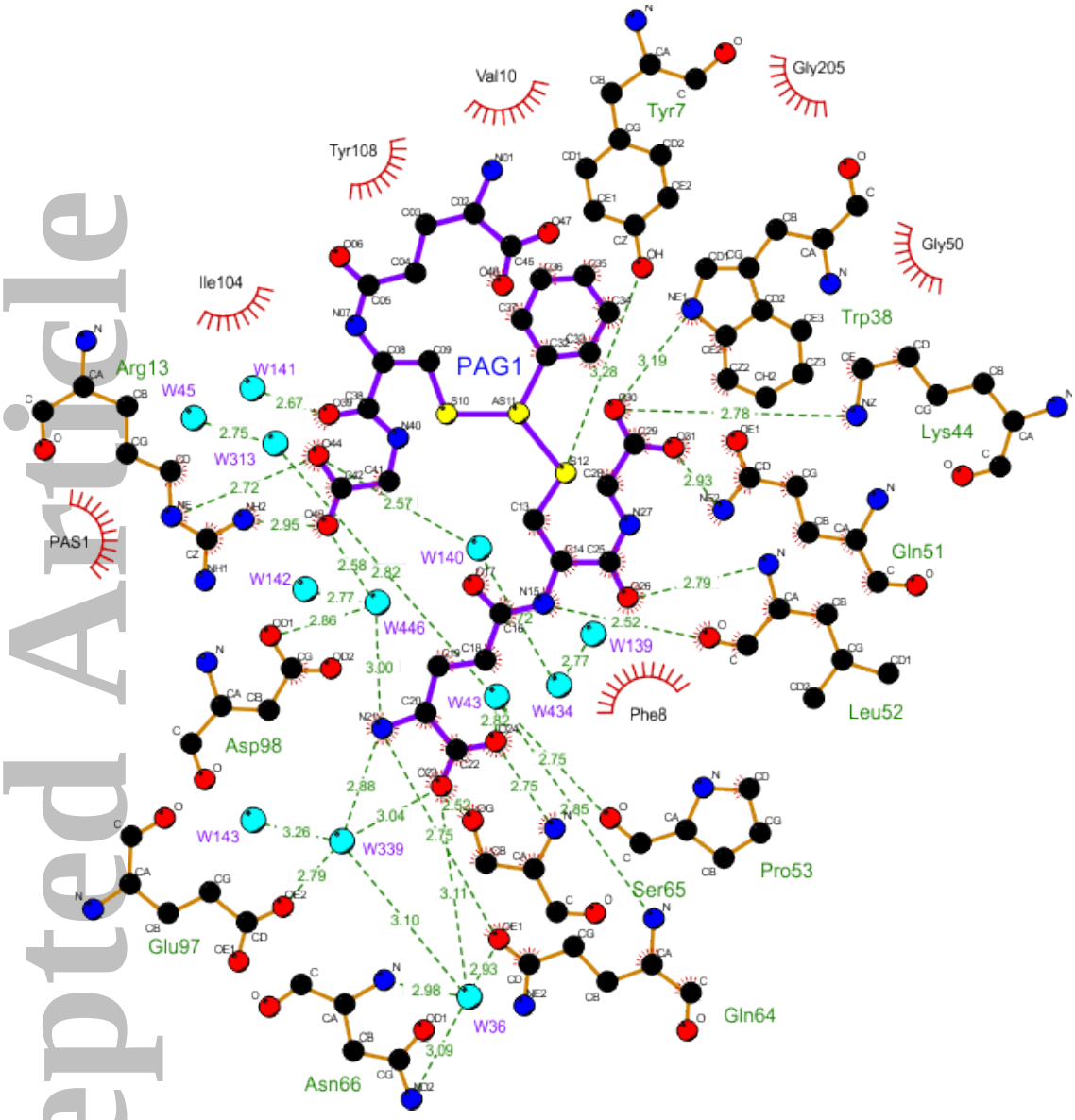

Figure S2. Diagrammatic representation of the interactions between GSTP1-1 and one of the bound di-GSH-phenylarsenic molecules (labeled as PAG1). Predicted hydrogen bonds are shown as dashed green lines with bond lengths indicated. Van der Waals interactions are shown as radiating lines. Figure produced with LIGPLOT [2].

John Wiley & Sons
This article is protected by copyright. All rights reserved.

Accepted Article

SUPPLEMENTAL MATERIALS AND METHODS

Related to main text Materials and Methods

Materials

Wild-type GSTP1-1, GSTP1-1 C47S, GSTP1-1 C101S and GSTP1-1 C476/C101S were expressed in *E. coli* and purified as described previously [3]. $PA(GS)_2$ was synthesized at three different concentrations of PAO (33, 66, and 100 μM final concentration) and GSH (1 mM final concentration) in 0.1 M potassium phosphate buffer pH 6.5 (25°C). $PA(GS)_2$ synthesis was followed by using a Kontron Uvikon-941 Plus (dual beam) spectrophotometer.

Kinetic Studies

The instability constant was calculated by adding step-by-step GSH (64 μM) to a fixed concentration of PAO (64 μM) in potassium phosphate buffer 0.1 M pH 6.5 and recording absorbance at 273 nm. Inhibition experiments of $PA(GS)_2$ on wild-type GSTP1-1, GSTP1-1 C47S, and GSTP1-1 C101S were performed by incubating 1 μg of enzyme in 0.1 M potassium phosphate buffer pH 6.5 (25°C) with variable amounts of GSH at fixed 1 mM CDNB at three different fixed $PA(GS)_2$ concentrations (0, 0.165, 0.66 and 1.65 μM). Reaction rates were recorded at 340 nm.

Fluorescence Study

The quenching of intrinsic fluorescence of wild-type GSP1-1, GSTP1-1 C47S, GSTP1-1 C101S, and GSP1-1 C47S/C101S (excitation wavelength 295 nm, emission wavelength 344 nm) was measured in a single photon counting spectrofluorometer Fluoromax-4 Horiba, with slits 5 nm, at 25°C, after the addition of variable amounts

John Wiley & Sons

This article is protected by copyright. All rights reserved.

Accepted Article

of PAO (from 3 to 60 μM; > 0.1 mM for C47S/C101S) and enzyme 1 μM in 0.1 M potassium phosphate buffer pH 6.5. Fluorescence data were corrected both for dilution and inner filter effect. Data were fitted according to allosteric curve fit:

$\Delta F = \Delta F_{max}/(1+K_L/[PAO]^{nH})$.

Crystallization

The wt human GSTP1-1 was expressed, purified and crystallized as described previously [4]. Crystals grew at 22 ˚C and reached a suitable size in approximately a week. Crystals were grown in either the presence or absence of GSH. Co-crystallization experiments were not attempted because DTT, an essential ingredient for crystallization, would react with PAO. (GST P1-1 crystals only grow in reducing conditions, likely due to the two highly reactive surface cysteines in each monomer of the GST dimer).

PAO was purchased from Sigma-Aldrich and was dissolved in DMSO to make a 20 mM stock solution. Aliquots of the stock were added to a reservoir solution and diluted to a final concentration of 0.2 – 2.0 mM PAO. Crystals were transferred to 2 μl drops and left to soak for periods of several hours to a week.

Data Collection, Structure Determination and Refinement

In total 12 data sets were collected from crystals soaked with varying concentrations of PAO for different time points and the best representative data sets from crystals grown in the presence or absence of GSH are described here. All crystals were cryoprotected in 5% (v/v) MPD for 30 seconds then transferred to 10% MPD for a further 30 seconds, before being plunged into liquid nitrogen.

John Wiley & Sons

This article is protected by copyright. All rights reserved.

Accepted Article

PAO soaked into crystals grown in the presence of GSH. The data set was collected at the Advanced Photon Source (Chicago, Illinois, USA) on BioCARS beam line 14-BM-C using an ADSC Quantum-315 CCD detector. The wavelength was set to 0.90 Å. A scan of the wavelength was done to confirm that arsenic was present in the crystals. A strong peak was observed at 11.87 KeV. Diffraction data were processed with MOSFLM [5] and scaled with the program SCALA [6]. Refinement began with the model of GSTP1-1 complexed to GSH (PDB id: 5GSS) after GSH and waters were removed. The test set of reflections was randomly generated using 5% of the data. Water and MES were added using COOT [7], interspersed by rounds of positional and isotropically restrained B-factor refinement using Phenix Refine [8].

Evidence that GSH and arsenic had bound was confirmed in the initial F_o-F_c difference Fourier map that showed large peaks for all ligands. The GSH thiols pointed towards each other, 3.9 Å apart, with a large F_o-F_c electron density peak (greater than 12σ) between them. This peak was also observed in an anomalous map at greater than 15σ and was thus interpreted as the arsenic atom. Two molecules of GSH per subunit were built in, covalently bound to the arsenic via the thiols. In addition, there was extra electron density radiating out from the arsenic atom that was interpreted as the phenyl ring of PAO. The G-site is fully occupied (GSH1) whereas the GSH molecule in the secondary binding site (GSH2) refined to an occupancy of 60% (together with the phenyl arsenic moiety), consistent with 40% of the enzyme molecules in the crystal being bound to GSH only. The phenyl arsenic molecule was built into the density in COOT [7]. Two additional strong F_o-F_c peaks (greater than 12σ) were identified at the dimer interface attached to the sulfur atoms of each C101. These were interpreted as two arsenic atoms and confirmed by peaks in corresponding positions in an anomalous difference Fourier map of greater than 15σ. The sites were

John Wiley & Sons
This article is protected by copyright. All rights reserved.

refined with occupancies of 0.6 and had an average *B*-factor of 26 Å^2, close to the B-factors of the C101 side-chains that had an average B-factor of 28 Å^2. There was some density attached to these arsenics that was modeled as the phenyl rings. The R_{cryst} for the final model is 18.0% (R_{free} of 21.3%) for all data to 1.5 Å resolution. A summary of the refinement statistics is given in Table S2. The model was analyzed with the program PROCHECK [9] which showed that its stereochemical quality was similar or better than expected for structures refined at similar resolutions.

PAO soaked into crystals grown in the absence of GSH. Diffraction data from a frozen GSTP1-1 crystal grown in the absence of GSH and soaked for 3 hrs in 2 mM PAO, were collected at the Australian Synchrotron on MX1 at 12 KeV near the absorption edge for arsenic, using an ADSC Quantum 210r Detector. Diffraction data were processed, scaled and the model refined as described above. Molecular replacement began with the model of GSTP1-1 complexed to GSH (PDB id: 5GSS) after GSH and waters were removed but was not successful, suggesting some movement of the subunits. Investigation of the unit cell dimensions revealed it had changed in two dimensions relative to the GSH complex: the *a* cell had decreased by 3.0 Å and the *b* cell edge increased by 5.3 Å (Table S2). The structure was subsequently solved by molecular replacement using PHASER [10] with a monomer of 5GSS (with all waters and ligands removed) as a probe. Several other data sets were also collected of this complex using both in-house and synchrotron radiation sources. The large change in unit cell dimensions was consistent across all data sets suggesting the change was due to PAO binding rather than an artifact of a cryocooling protocol, which was performed in the same manner for all crystals, with and without GSH.

Accepted Article

John Wiley & Sons
This article is protected by copyright. All rights reserved.

There were two weak peaks, ~ 5σ in the first difference F_o-F_c map, attached to the C101 of each subunit (Fig. 3*A*). These two peaks were modeled as low occupancy arsenic atoms and there was no density for other metalloid ligands associated with the cysteine residues. (Data sets were collected from GSTP1-1 crystals soaked in PAO solutions between 3 and 24 hours and the amount of metalloid bound did not appear to increase with the longer soak times). Calculation of an anomalous difference Fourier map, using Anode [11] (CCP4), revealed peaks of 12σ at these same positions, confirming the location of the metalloid ions. In all data sets collected from crystals grown in the absence of GSH, the region corresponding to helix α2, residues 35-50, is missing in the electron density in both subunits. The R_{cryst} for the final model was 15.7% (R_{free} of 20.4%) for all data to 2.1 Å resolution. A considerable number of waters observed in the GSH complex structure were not seen in this structure (Table S2) due to the widening of the dimer interface and subsequent loss of networks of water molecules that bridged the interface. A summary of the refinement statistics is given in Table S2. The model was analyzed with the program PROCHECK [9] which showed that the stereochemical quality was similar or better than expected for structures refined at similar resolutions.

PAO soaked into GSTP1-1 crystals grown in the absence of GSH and then back-soaked with GSH. Crystals from the same drop as the PAO in the absence of GSH experiment described above were transferred into well solution containing 10 mM GSH after 2 days. They were left to soak for 5 days. Data were collected at the Australian Synchrotron, on the MX1 beamline, at 12 KeV, as described above. Diffraction data were processed and scaled and the structure determined and refined as described above. Evidence that GSH and arsenic had bound was confirmed in the

John Wiley & Sons
This article is protected by copyright. All rights reserved.

initial F_o-F_c difference Fourier map that showed large peaks for all ligands. The di-GSH-phenyl-arsenic complex was built in as described above. Calculation of an anomalous difference Fourier map, using Anode [11] (CCP4), revealed peaks of 23 σ between the thiols of the two GSH molecules in each active site. Unlike the PAO-GSH structure described above, there were no peaks, anomalous or other, connected to the C101 thiols. The R_{cryst} for the final model is 14.1% (R_{free} of 17.2%) for all data to 2.0 Å resolution. A summary of the refinement statistics is given in Table S2.

Apo GSTP1-1. Crystals grown in the absence of GSH or ligand were collected in-house at 100 K and recorded on a Rigaku R-AXIS IV++ imaging plate area detector (Rigaku, Japan) using a Rigaku MicroMax^{TM}-007HF microfocus rotating anode generator (Rigaku, Japan) as an X-ray source. The data were processed using the program MOSFLM [5] and AIMLESS [12]. The structure was determined and refined as described above. The R_{cryst} for the final model is 14.6% (R_{free} of 18.3%) for all data to 2.0 Å resolution. A summary of the refinement statistics is given in Table S2.

XAS Studies

XAS experiments were undertaken to determine the immediate environment of the arsenic after incubation of PAO with GSTP1-1. These experiments were only done in the absence of GSH since GSH reacts with PAO directly. GSTP1-1 was incubated with PAO for various lengths of time and at various concentrations to optimize the binding of the metalloid at a single site. The solutions were analyzed by mass spectrometry on an Agilent 6510 Q-TOF LC/MS (Bio21 Institute, Melbourne University). Results from the mass spectrometry suggested that interaction of PAO with the protein at a single site per monomer was optimal at 2:1 ratio of PAO for 10

John Wiley & Sons
This article is protected by copyright. All rights reserved.

hrs. A 4 ml solution of 0.11 mM PAO was incubated with 0.05 mM GST for 10 hrs and then concentrated to 400 μl (protein concentration of ~ 1 mM, in phosphate buffered saline, pH 6.5). Any unbound PAO was dialyzed away prior to flash-freezing the sample in an isopentane/liquid nitrogen slurry. Due to the low concentration of arsenic in the samples, 12 repeat EXAFS scans to k = 12 $Å^{-1}$ were conducted over a 12 hr period. XAS data were recorded at 20 K on beamline 20B at the Photon Factory (Tsukuba, Japan). K-edge As XAS were measured in fluorescence detection mode using a 36-element Ge monolithic pixel array detector (Eurisys). All data were collected using a Si[111] double monochromator, detuned to 50% to effect harmonic rejection. Energy calibration was achieved by simultaneously recording the transmission spectrum of solid sodium arsenate diluted in boron nitride, downstream of the sample, whose white line peak energy was assumed to be 11,874.7 eV.

Mass Spectrometry Studies

Post complex formation, DTT and excess complex were dialyzed away using the storage buffer (without DTT). Reaction mixtures were analyzed by electrospray mass spectrometry on an Agilent 6510 Q-TOF LC/MS (Bio21 Institute, Melbourne University) with the following settings: fragmentor at 215 V, skimmer at 65 V and capillary voltage at 4000 V. Spectra were deconvoluted using Agilent MassHunter 5.

Accepted Article

John Wiley & Sons

This article is protected by copyright. All rights reserved.

SUPPLEMENTAL REFERENCES

1. Chen VB, Arendall WB, 3rd, Headd JJ, Keedy DA, Immormino RM, Kapral GJ, Murray LW, Richardson JS, Richardson DC (2010) MolProbity: all-atom structure validation for macromolecular crystallography. Acta Crystallogr D Biol Crystallogr 66:12-21.

2. Wallace AC, Laskowski RA, Thornton JM (1995) LIGPLOT: a program to generate schematic diagrams of protein-ligand interactions. Protein Eng 8:127-134.

3. Lo Bello M, Battistoni A, Mazzetti AP, Board PG, Muramatsu M, Federici G, Ricci G (1995) Site-directed mutagenesis of human glutathione transferase P1-1. Spectral, kinetic, and structural properties of Cys-47 and Lys-54 mutants. J Biol Chem 270:1249-1253.

4. Parker LJ, Ciccone S, Italiano LC, Primavera A, Oakley AJ, Morton CJ, Hancock NC, Bello ML, Parker MW (2008) The anti-cancer drug chlorambucil as a substrate for the human polymorphic enzyme glutathione transferase P1-1: kinetic properties and crystallographic characterisation of allelic variants. J Mol Biol 380:131-144.

5. Leslie AW, Powell H. Processing diffraction data with mosflm. In: Read R, Sussman J, editors. Evolving Methods for Macromolecular Crystallography. Volume 245, NATO Science Series: Springer Netherlands; 2007. p 41-51.

6. Collaborative Computational Project N (1994) The CCP4 Suite: Programs for Protein Crystallography. Acta Crystallogr D 50:760-763.

7. Emsley P, Cowtan K (2004) Coot: model-building tools for molecular graphics. Acta Crystallographica Section D-Biological Crystallography 60:2126-2132.

Accepted Article

John Wiley & Sons

This article is protected by copyright. All rights reserved.

8. Adams PD, Afonine PV, Bunkoczi G, Chen VB, Davis IW, Echols N, Headd JJ, Hung LW, Kapral GJ, Grosse-Kunstleve RW and others (2010) PHENIX: a comprehensive Python-based system for macromolecular structure solution. Acta Crystallogr D Biol Crystallogr 66:213-221.

9. Laskowski RA, MacArthur MW, Moss DS, Thornton JM (1993) PROCHECK: a program to check the stereochemical quality of protein structures. Journal of Applied Crystallography 26:283-291.

10. McCoy AJ, Grosse-Kunstleve RW, Adams PD, Winn MD, Storoni LC, Read RJ (2007) Phaser crystallographic software. J Appl Crystallogr 40:658-674.

11. Thorn A, Sheldrick GM (2011) ANODE: anomalous and heavy-atom density calculation. J Appl Crystallogr 44:1285-1287.

12. Evans PR, Murshudov GN (2013) How good are my data and what is the resolution? Acta Crystallogr D Biol Crystallogr 69:1204-1214.

Accepted Article

John Wiley & Sons

This article is protected by copyright. All rights reserved.

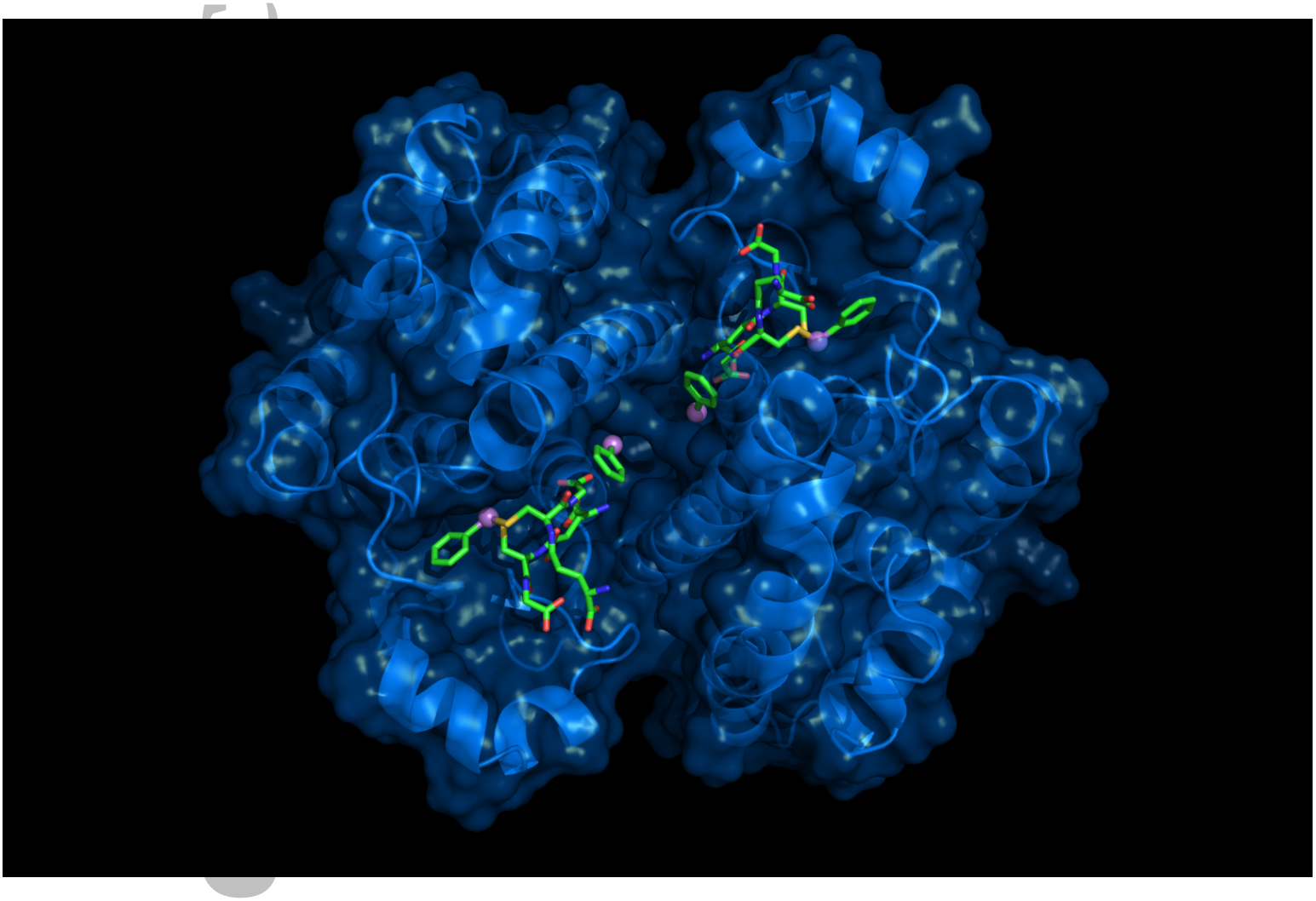

John Wiley & Sons
This article is protected by copyright. All rights reserved.

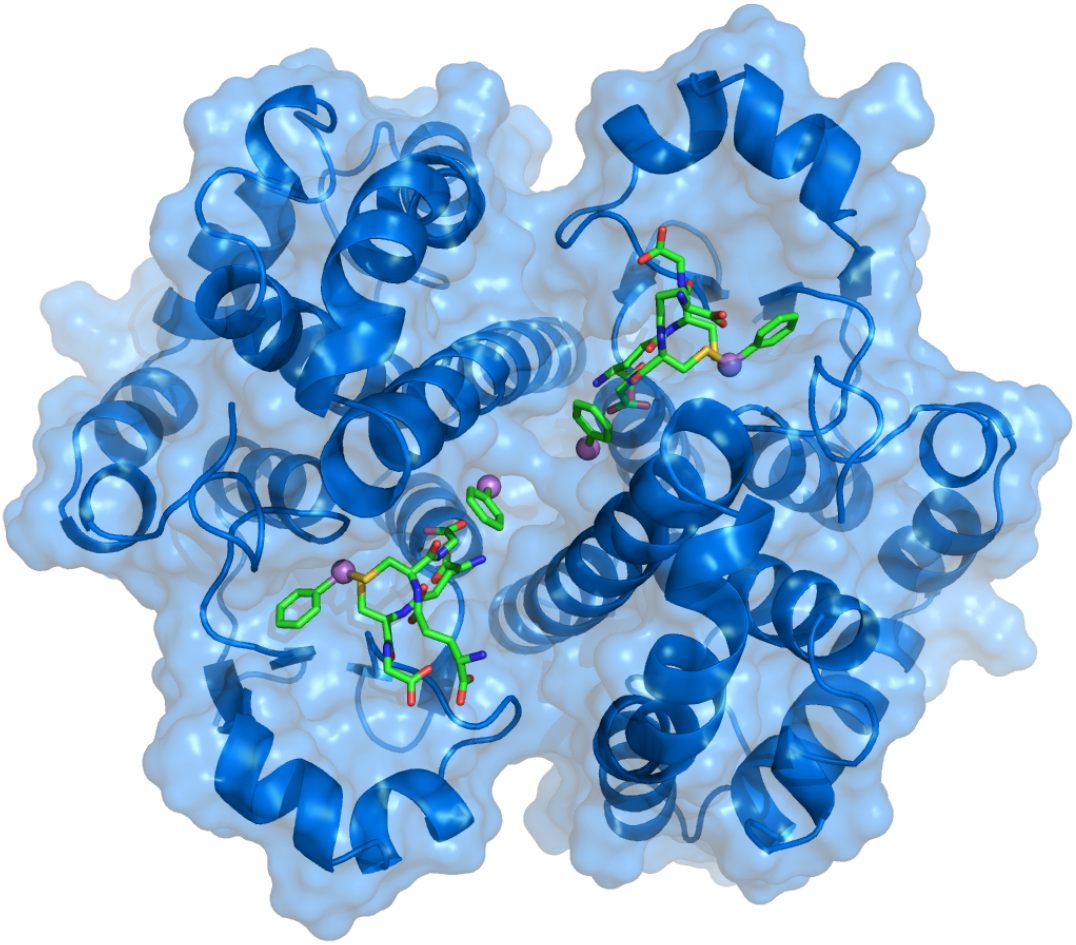

John Wiley & Sons
This article is protected by copyright. All rights reserved.